

# High-order harmonic generation from field-distorted orbitals

Maciej Dominik Śpiewanowski, Adam Etches, and Lars Bojer Madsen

*Department of Physics and Astronomy, Aarhus University, DK-8000 Aarhus C, Denmark*

(Dated: April 25, 2022)

We investigate the effect on high-order harmonic generation of the distortion of molecular orbitals by the driving laser field. Calculations for high-order harmonic generation including orbital distortion are performed for N<sub>2</sub>. Our results allow us to suggest that field-distortion is the reason why the two-center interference minimum has never been observed experimentally in N<sub>2</sub>. We propose experimental parameters which should allow an observation of the two-center interference minimum.

PACS numbers: 33.20.Xx,42.65.Ky,42.50.Hz

## I. INTRODUCTION

During the last decades, high-order harmonic generation (HHG) has been subject to extensive experimental and theoretical studies. Apart from being a source of coherent XUV radiation [1, 2], and ultrafast pulses [3–5], the process of HHG has also been used to extract internuclear separations [6–9] and electronic orbitals [10–14]. The intrinsic timing in the HHG process associated with the time from ionization to recombination can, e.g., be used to resolve nuclear dynamics on an ultrafast timescale [6–8]. Turning to orbital tomography, the HHG signal has been used to reconstruct molecular orbitals: the highest occupied molecular orbital (HOMO) in N<sub>2</sub> [10–13], the HOMO-1 in N<sub>2</sub> [13], the HOMO in CO<sub>2</sub> [12, 14] and the HOMO in O<sub>2</sub> [12]. Given the experimental laser intensities, it is surprising that, in all of these cases, there has been no measurable signature of field-distortion in the reconstructed orbitals. The present work identifies for the first time a clear signature of significant field-induced orbital distortion in the HHG process by focusing on the effect of the distortion on the two-center interference minimum [15–18]. Indeed, one of the most prominent features of an HHG spectrum is the presence of a minimum. Such a minimum may have different origin depending on the target and laser parameters, but it always carries important information about the target. For example, a Cooper minimum holds information about the electronic structure of the target [19–23]. Participation of multiple orbitals in the HHG process gives rise to a so-called dynamic minimum which allows elucidation of the interplay between the HOMO and lower-lying orbitals in the HHG process [24, 25]. Finally, a two-center interference minimum gives access to structural information [15–18].

Accounting for the effects of orbital distortion allows us to resolve a long-disputed puzzle in N<sub>2</sub>: Both experimental and theoretical works have proven the existence of Cooper minima [19–23, 26] and the role of multiple molecular orbital contributions in HHG spectra [27]. Yet the two-center interference minimum, though theoretically predicted [28, 29], has never been observed experimentally [10, 23, 30]. We explain the lack of a two-center interference minimum in terms of laser-induced orbital

distortion. We also show that for specific field parameters and orientation of the molecule it should be possible to observe experimentally the two-center minimum in the long trajectories of the HHG spectrum.

## II. MODEL

We assume that the electronic structure of the molecule adiabatically adjusts to the time-varying external field,  $\mathbf{F}(t)$ . With this assumption the Lewenstein model [31] is extended to include not only the Stark shift [32], but also the field-distortion of the initial and final states. For sake of clarity we present the approach with participation of only the HOMO in the HHG process (the methodology can be straightforwardly extended to include more orbitals). The HHG spectrum along the polarization  $\epsilon$  can then be calculated as [33]

$$S_{\epsilon}(\omega) = \left| \int_{-\infty}^{\infty} \epsilon \cdot \langle \hat{\mathbf{v}}(t) \rangle e^{i\omega t} dt \right|^2, \quad (1)$$

where the expectation value of the dipole velocity operator reads

$$\langle \hat{\mathbf{v}}(t) \rangle = -i \int_{-\infty}^t dt' \int_{\mathbb{R}^3} d\mathbf{k} M_{\text{rec}}(t) e^{-iS(\mathbf{k}, t, t')} M_{\text{ion}}(t') + c.c., \quad (2)$$

with

$$M_{\text{ion}}(t') = \langle \psi_{\mathbf{k}}^{\text{V}}(t') | V_{\text{L}}(t') | \psi(\mathbf{F}(t')) \rangle \quad (3)$$

the ionization matrix element,

$$S(\mathbf{k}, t, t') = \int_{t'}^t \frac{1}{2} (\mathbf{k} + \mathbf{A}(t''))^2 dt'' - \int_{t'}^t E(t'') dt'' \quad (4)$$

the phase accumulated while the electron propagates from time  $t'$  to  $t$ , and

$$M_{\text{rec}}(t) = \langle \psi(\mathbf{F}(t)) | \hat{\mathbf{v}} | \psi_{\mathbf{k}}^{\text{V}}(t) \rangle, \quad (5)$$

the recombination matrix element. The Stark-shifted HOMO energy is denoted by  $E(t)$  in Eq. (4). Using perturbation theory  $E(t) = E_0 - \boldsymbol{\mu} \cdot \mathbf{F}(t) - 1/2 \mathbf{F}(t)^{\text{T}} \underline{\underline{\alpha}} \mathbf{F}(t)$  with  $E_0$  the field-free HOMO energy,  $\boldsymbol{\mu}$  the dipole of the

HOMO and  $\underline{\alpha}$  the polarizability tensor. In Eqs. (3) and (5) the HOMO  $|\psi(\mathbf{F}(t))\rangle$  depends explicitly on the instantaneous value of the driving laser field  $\mathbf{F}(t)$ . Propagation of the continuum electron with momentum  $\mathbf{k}$  is described by the Volkov state  $|\psi_{\mathbf{k}}^V(t)\rangle$ , and  $V_L(t) = \mathbf{F}(t) \cdot \mathbf{r}$  describes the interaction with the laser field. We obtain initial and final states by calculating field-dependent orbitals with quantum chemistry methods [34] using an aug-cc-pTZV basis set [35, 36]. This approach was successfully used to study deformations in CO<sub>2</sub> molecules subject to even stronger fields than used here [37]. To obtain the spectrum, the field-distorted orbitals and corresponding energies are calculated at every time step needed for an accurate evaluation of the integral in Eq. (2). This approach incorporates many-electron effects on the bound state since the calculation of molecular orbitals exposed to the laser field involves the multielectron response. We note that the present approach requires that the distorted orbitals are calculated at the instantaneous value of the external field. Hence, the approach refers to a description using the length gauge for the electron-laser interaction, which allows the usage of standard quantum chemistry program packages for static-field calculations. The HOMO obtained in this way may be transferred to the velocity gauge by a suitable unitary transformation [38].

### III. RESULTS

We freeze the nuclei in N<sub>2</sub> at the internuclear distance of 2.08 a.u. and set the ionization potential to 15.56 eV. The molecule is aligned [39] at  $\beta = 75^\circ$  with respect to the polarization axis of a linearly polarized driving pulse. The pulse has a five-cycle trapezoidal envelope with one optical cycle for ramp-up and -down. The peak intensity is  $9 \times 10^{13}$  W/cm<sup>2</sup>, and the carrier wave length is 1300 nm. For this orientation and intensity it can be safely assumed that multiple orbital contributions are negligible (see Ref. [27]) and therefore we restrict ourselves to the signal emitted by electrons detached from the HOMO. Possible depletion effects (not treated here) are not expected to affect the shape of the HHG spectra, but only the overall yield, and will, hence, not alter our main conclusions.

When field-free HOMOs are used in the ionization [Eq. (3)] and recombination [Eq. (5)] steps the model reduces to that of Ref. [32], i.e., the Lewenstein model [31] including Stark shifts. This model predicts a two-center interference minimum at  $\sim 58$  eV [Fig. 1(a)]. The minimum is identified as a two-center interference minimum by its change in position when varying the alignment angle: We have checked that the minimum moves to higher photon energy when increasing the alignment angle [15, 16, 29]. Such a minimum has never been observed experimentally (see, e.g., Refs. [10, 30]), irrespective of orientation and laser intensity. The two-center interference minimum of concern should not be confused with

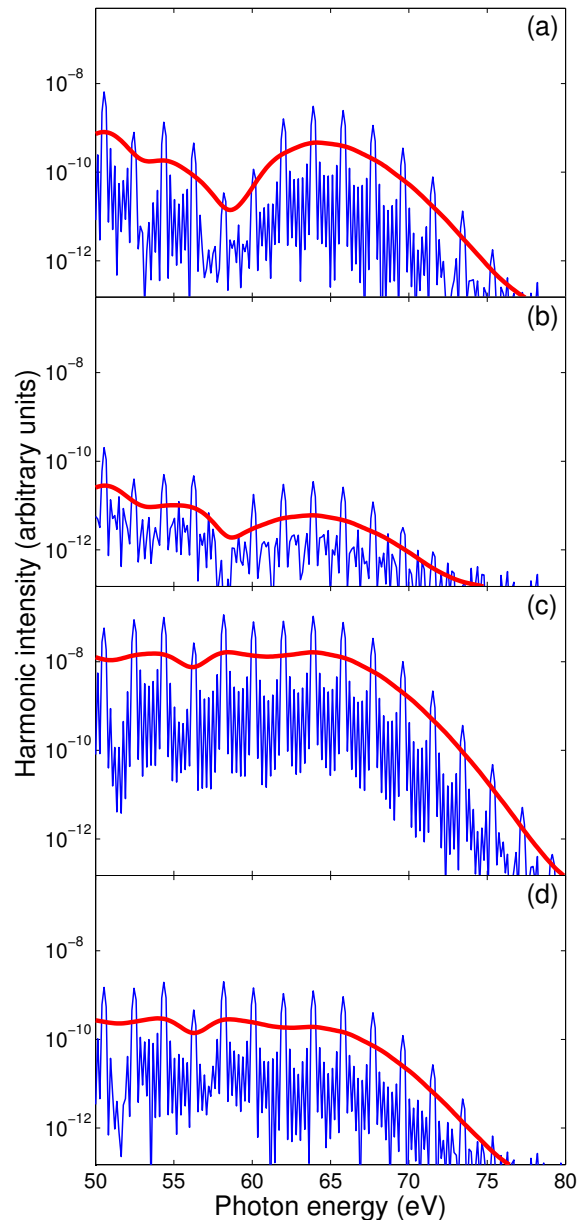


FIG. 1: (Color online) HHG spectra for N<sub>2</sub> (see text for laser parameters and orientation). The thick (red) curves indicate spectra smoothed with a Gaussian distribution with full-width-half-maximum of 4 harmonics. (a) Field-free HOMO in ionization [see Eq. (3)] and recombination [see Eq. (5)] steps. (b) Field-distorted HOMO in ionization and field-free HOMO in recombination steps. (c) Field-free HOMO in ionization and field-distorted HOMO in recombination steps. (d) Field-distorted HOMO in ionization and recombination steps.

the Cooper minimum, which appears at  $\sim 38$  eV [23, 26]. The latter minimum is related to scattering properties of the molecular potential [40] and is not considered in the present work, where we focus at larger energies, where the approach treating the continuum states as Volkov waves is reasonably accurate. Next we use a field-distorted

HOMO in the ionization matrix element, leaving the state in the recombination matrix element field-free. The two-center interference minimum remains visible in the spectrum [Fig. 1(b)], and hence we reach the conclusion that the deformation of the initial state does not significantly obscure the structural information associated with the two-center minimum. An important change as compared with Fig. 1(a) is a much lower yield which is caused by destructive interference between amplitudes originating from different ionization times. In the next step we examine the role of the recombination matrix element [see Eq.(5)] and use a field-distorted HOMO in the recombination, and a field-free HOMO in the ionization step. The result is depicted in Fig. 1(c). The disappearance of the minimum proves that the recombination matrix element is sensitive to orbital distortion, and in this sense holds structural information about the target. Similarly, the minimum disappears when taking into account the field-distortion of the HOMO in both the ionization and recombination steps [Fig. 1(d)].

The two-center interference minimum appears when the recombination matrix elements on both atomic centers are of similar magnitude and their phase difference is  $\pi$ . To calculate the recombination matrix element on a given center we use that the orbitals are expanded in atomic centered Gaussian basis functions and take the part of the molecular orbital centered on the atomic center of interest [41]. In Fig. 2 we show how orbital distortion significantly changes the relative strengths and phases. If the HOMO is field-free in the recombination step [Figs. 1(a) and (b)], then the norms of recombination matrix elements on both centers are equal as shown in Fig. 2(a). The phase difference reaches  $\pi$  for a continuum electron energy of  $\sim 42$  eV corresponding, by adding the ionization potential, to a harmonic energy of  $\sim 58$  eV. This explains the position of the minima in Figs. 1(a) and (b). When taking into account field-distortion in the recombination step the value of the field changes with recombination time. In Figs. 2(b) and (c) we depict the norm and phase of the recombination matrix elements when the HOMO is distorted by  $F = 0.01$  a.u. and  $F = 0.04$  a.u., respectively. These figures show that the norms on different centers become increasingly different for increasing field. As a consequence the two-center interference minimum weakens and subsequently totally vanishes. Monitoring the variation of the minimum with the field strength allows us to specify a range of field values for which observation of the minimum is possible. This range corresponds to recombination at fields  $|F| \lesssim 0.012$  a.u., and we will refer to it as the weak-field region.

While Fig. 2 defines the weak-field region, it does not contain information about the value of the field at the time of recombination. To this end we consider a time-profile analysis [42–44]. Figure 3 presents such an analysis corresponding to the spectra in Figs. 1(a) and 1(d). The figure shows which recombination, i.e., emission times contribute to the signal at a given photon en-

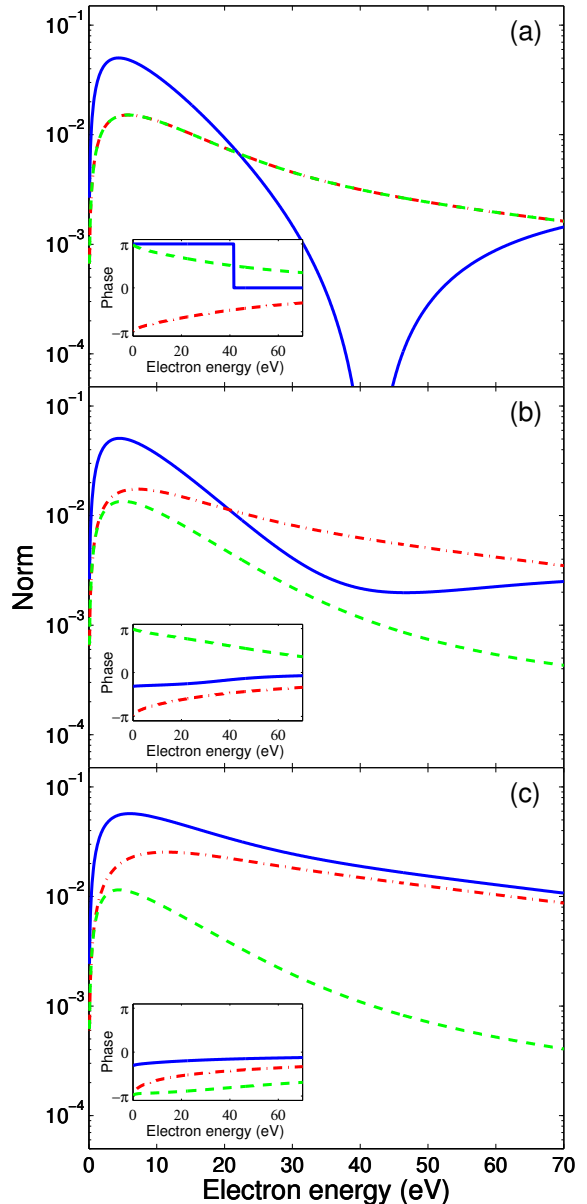


FIG. 2: (Color online) Norm and phase (inserts) of recombination matrix elements [Eq. (5)] for (a)  $F = 0$  a.u., (b)  $F = 0.01$  a.u., (c)  $F = 0.04$  a.u. The full (blue) curves show results using the field-distorted HOMO, dot-dashed (red) curves denote field-distorted recombination on the N atom at the negative  $z$  axis in the molecular frame, and dashed (green) denote field-distorted recombination on the N atom at the positive  $z$  axis in the molecular frame.

ergy. Figures 3(a) and (c) show that the harmonics come in bursts each half cycle. Each harmonic burst consists of two branches, known as the short and long trajectories [45]. The short trajectories start less than  $2/3$  of an optical cycle before recombination and give rise to branches with positive slope. The long trajectories start

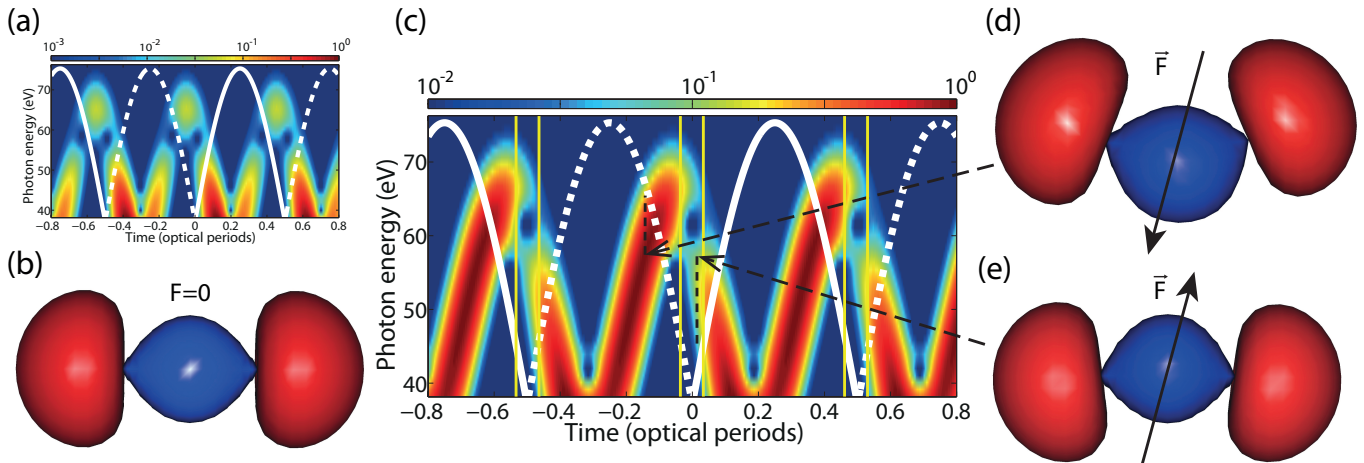


FIG. 3: (Color online) Emission times of the spectra presented in Figs. 1(a) and 1(d). (a) Emission times when performing the calculation with undistorted HOMOs in the ionization and recombination steps [Fig. 1(a)]. Curves indicate positive (full, white) and negative (dashed, white) values of the laser field at the recombination time. (b) Field-free, undistorted HOMO. (c) Emission times when performing the calculation with field-distorted HOMOs in the ionization and recombination steps [Fig. 1(d)]. Curves indicate positive (full, white) and negative (dashed, white) values of the laser field at the recombination time. The vertical (yellow) lines identify the weak-field regions (see text). (d) Field-distorted HOMO for  $F = 0.04$  a.u.. (e) Field-distorted HOMO for  $F = 0.01$  a.u.. In (d) and (e) full (black) arrows indicate the field direction. The arrows from (d), and (e) to (c) indicate the recombination times for which the HOMOs are depicted, and dashed (black) lines in (c) guide the eye to the corresponding value of the field.

more than  $2/3$  of an optical cycle before recombination, and give rise to branches with negative slope. Figure 3(a) shows that when the calculation is performed using the undistorted HOMO shown in Fig. 3(b), there is a minimum at around 58 eV in both branches, consistent with the minimum in Fig. 1(a). Figure 3(c) shows that when field-distortion is included (see Figs. 3(d) and 3(e) for snapshots of the distorted orbitals), the short trajectory branches are more intense than the long trajectory branches, and no minima occur in the former. For example, the short trajectory branches give rise to photons at 61 eV while the corresponding long trajectory branches do not contribute significantly to this photon energy. In Fig. 3(c) the vertical (yellow) lines indicate the time windows where the field at recombination is within the weak-field region. We see that the trajectories that recombine in these windows belong to the long trajectory branches. The minimum at 61 eV for the long trajectory branch is the two-center interference minimum, that is shifted in position by orbital-distortion from 58 eV in the undistorted case [Fig. 3(a)]. Following the discussion in connection with Fig. 2, this implies that the two-center interference minimum can only be observed in the long trajectory branch, and therefore a measurement isolating the contribution to the spectrum from the long trajectories may lead to an observation of a two-center interference minimum in  $N_2$ .

The reason why the minimum is not seen in Fig. 1(d) is that the short trajectory harmonics dominate the spec-

trum in our calculation (see Fig. 3). To isolate the spectrum originating from the long trajectories, macroscopic phase matching should be used to select the long trajectories by either changing the focusing conditions of the driving field [46] or by far-field separation [47] (see also the review [45] and references therein).

#### IV. CONCLUSION AND OUTLOOK

Our results indicate that field-distortion of molecular orbitals can be important for understanding spectral features of molecular targets. The effect of orbital distortion is manifested in both ionization and recombination events. The orbital distortion in the ionization event results in a lower HHG yield in  $N_2$  compared to the undistorted case. Orbital distortion in the recombination step influences the structural information encoded in the spectrum. For example, the absence of a two-center interference minimum in the HHG spectrum of  $N_2$  is a clear signature of orbital distortion taking place when the short trajectory recombines outside the weak-field limit. By carefully adjusting the molecular orientation and the laser parameters, conditions can be obtained such that the long trajectory recombines within the weak-field limit, allowing the observation of the  $N_2$  two-center interference minimum.

The field-distorted orbitals can be obtained in standard quantum chemistry software packages [34], and

therefore the methodology can be applied to many molecular systems. The approach opens up the possibility to study a range of questions that can shed more light on the process of HHG. For example, the effect of the orbital distortion will be very sensitive to the value of the polarizability.  $N_2$  has a relatively high polarizability, and therefore the effect on the spectrum is large. In other systems, for example  $CO_2$ , the polarizability is much smaller, and orbital distortion should be less important. In addition, an approach including orbital distortion is highly relevant for orbital tomography. Our work indicates that HHG-based orbital tomography will never allow the reconstruction of a field-free orbital, but rather gives a coherent average over field-distorted orbitals. The degree

of field-distortion may be reduced by using short driving pulses [48], and isolating the contribution from the long trajectories. Finally, we note that the present approach can also be used to address the effect of orbital-distortion in the strong-field approximation for ionization [49–51].

### Acknowledgments

This work was supported by the Danish Center for Scientific Computation, the Danish Natural Science Research Council, and an ERC-StG (Project No. 277767 - TDMET).

- 
- [1] A. Rundquist, C. G. Durfee, Z. Chang, C. Herne, S. Backus, M. M. Murnane, and H. C. Kapteyn, *Science* **280**, 1412 (1998).
- [2] R. Bartels, S. Backus, E. Zeek, L. Misoguti, G. Vdovin, I. Christov, M. Murnane, H. Kapteyn, et al., *Nature* **406**, 164 (2000).
- [3] M. Drescher, M. Hentschel, R. Kienberger, G. Tempea, C. Spielmann, G. A. Reider, P. B. Corkum, and F. Krausz, *Science* **291**, 1923 (2001).
- [4] M. Hentschel, R. Kienberger, C. Spielmann, G. Reider, N. Milosevic, T. Brabec, P. Corkum, U. Heinzmann, M. Drescher, and F. Krausz, *Nature* **414**, 509 (2001).
- [5] G. Sansone, E. Benedetti, F. Calegari, C. Vozzi, L. Avaldi, R. Flammini, L. Poletto, P. Villoresi, C. Altucci, R. Velotta, et al., *Science* **314**, 443 (2006).
- [6] S. Baker, J. S. Robinson, C. A. Haworth, H. Teng, R. A. Smith, C. C. Chirilă, M. Lein, J. W. G. Tisch, and J. P. Marangos, *Science* **312**, 424 (2006).
- [7] S. Baker, J. S. Robinson, M. Lein, C. C. Chirilă, R. Torres, H. C. Bandulet, D. Comtois, J. C. Kieffer, D. M. Villeneuve, J. W. G. Tisch, et al., *Phys. Rev. Lett.* **101**, 053901 (2008).
- [8] W. Li, X. Zhou, R. Lock, S. Patchkovskii, A. Stolow, H. C. Kapteyn, and M. M. Murnane, *Science* **322**, 1207 (2008).
- [9] X. Zhou, R. Lock, W. Li, N. Wagner, M. M. Murnane, and H. C. Kapteyn, *Phys. Rev. Lett.* **100**, 073902 (2008).
- [10] J. Itatani, J. Levesque, D. Zeidler, H. Niikura, H. Pépin, J. C. Kieffer, P. B. Corkum, and D. M. Villeneuve, *Nature* **432**, 867 (2004).
- [11] S. Patchkovskii, Z. Zhao, T. Brabec, and D. M. Villeneuve, *Phys. Rev. Lett.* **97**, 123003 (2006).
- [12] S. Patchkovskii, Z. Zhao, T. Brabec, and D. Villeneuve, *J. Chem. Phys.* **126**, 114306 (2007).
- [13] S. Haessler, J. Caillat, W. Boutu, C. Giovanetti-Teixeira, T. Ruchon, T. Auguste, Z. Diveki, P. Breger, A. Maquet, B. Carré, et al., *Nature Physics* **6**, 200 (2010).
- [14] C. Vozzi, M. Negro, F. Calegari, G. Sansone, M. Nisoli, S. De Silvestri, and S. Stagira, *Nature Physics* **7**, 822 (2011).
- [15] M. Lein, N. Hay, R. Velotta, J. P. Marangos, and P. L. Knight, *Phys. Rev. Lett.* **88**, 183903 (2002).
- [16] M. Lein, N. Hay, R. Velotta, J. P. Marangos, and P. L. Knight, *Phys. Rev. A* **66**, 023805 (2002).
- [17] T. Kanai, S. Minemoto, and H. Sakai, *Nature* **435**, 470 (2005).
- [18] C. Vozzi, F. Calegari, E. Benedetti, J.-P. Caumes, G. Sansone, S. Stagira, M. Nisoli, R. Torres, E. Heesel, N. Kajumba, et al., *Phys. Rev. Lett.* **95**, 153902 (2005).
- [19] A. L’Huillier and P. Balcou, *Phys. Rev. Lett.* **70**, 774 (1993).
- [20] J. Farrell, B. McFarland, M. Gühr, and P. Bucksbaum, *Chem. Phys.* **366**, 15 (2009).
- [21] B. K. McFarland, J. P. Farrell, P. H. Bucksbaum, and M. Gühr, *Phys. Rev. A* **80**, 033412 (2009).
- [22] J. Higuier, H. Ruf, N. Thiré, R. Cireasa, E. Constant, E. Cormier, D. Descamps, E. Mével, S. Petit, B. Pons, et al., *Phys. Rev. A* **83**, 053401 (2011).
- [23] J. B. Bertrand, H. J. Wörner, P. Hockett, D. M. Villeneuve, and P. B. Corkum, *Phys. Rev. Lett.* **109**, 143001 (2012).
- [24] O. Smirnova, Y. Mairesse, S. Patchkovskii, N. Dudovich, D. Villeneuve, P. Corkum, and M. Ivanov, *Nature* **460**, 972 (2009).
- [25] E. P. Fowe and A. D. Bandrauk, *Phys. Rev. A* **81**, 023411 (2010).
- [26] H. J. Wörner, J. B. Bertrand, P. Hockett, P. B. Corkum, and D. M. Villeneuve, *Phys. Rev. Lett.* **104**, 233904 (2010).
- [27] C. Jin, J. B. Bertrand, R. R. Lucchese, H. J. Wörner, P. B. Corkum, D. M. Villeneuve, A.-T. Le, and C. D. Lin, *Phys. Rev. A* **85**, 013405 (2012).
- [28] B. Zimmermann, M. Lein, and J. M. Rost, *Phys. Rev. A* **71**, 033401 (2005).
- [29] S. Odžak and D. B. Milošević, *Phys. Rev. A* **79**, 023414 (2009).
- [30] Y. Mairesse, J. Levesque, N. Dudovich, P. B. Corkum, and D. M. Villeneuve, *Journal of Modern Optics* **55**, 2591 (2008).
- [31] M. Lewenstein, P. Balcou, M. Y. Ivanov, A. L’Huillier, and P. B. Corkum, *Phys. Rev. A* **49**, 2117 (1994).
- [32] A. Etches and L. B. Madsen, *J. Phys. B* **43**, 155602 (2010).
- [33] J. C. Baggesen and L. B. Madsen, *J. Phys. B* **44**, 115601 (2011).
- [34] M. W. Schmidt, K. K. Baldrige, J. A. Boatz, S. T. Elbert, M. S. Gordon, J. H. Jensen, S. Koseki, N. Matsunaga, K. A. Nguyen, S. Su, et al., *J. Comput. Chem.*

- 14**, 1347 (1993).
- [35] T. H. Dunning, Jr., *J. Chem. Phys.* **90**, 1007 (1989).
- [36] R. A. Kendall, T. H. Dunning, Jr., and R. Harrison, *J. Chem. Phys.* **96**, 6796 (1992).
- [37] H. Kono, S. Koseki, M. Shiota, and Y. Fujimura, *J. Phys. Chem. A* **105**, 5627 (2001).
- [38] L. B. Madsen, *Phys. Rev. A* **65**, 053417 (2002).
- [39] H. Stapelfeldt and T. Seideman, *Rev. Mod. Phys.* **75**, 543 (2003).
- [40] H. J. Wörner, H. Niikura, J. B. Bertrand, P. B. Corkum, and D. M. Villeneuve, *Phys. Rev. Lett.* **102**, 103901 (2009).
- [41] A. Etches, M. B. Gaarde, and L. B. Madsen, *Phys. Rev. A* **84**, 023418 (2011).
- [42] P. Antoine, B. Piraux, and A. Maquet, *Phys. Rev. A* **51**, R1750 (1995).
- [43] G. Kamta and A. D. Bandrauk, *Phys. Rev. A* **70**, 011404 (2004).
- [44] C. C. Chirilă, I. Dreissigacker, E. V. van der Zwan, and M. Lein, *Phys. Rev. A* **81**, 033412 (2010).
- [45] M. B. Gaarde, J. L. Tate, and K. J. Schafer, *J. Phys. B* **41**, 132001 (2008).
- [46] P. Antoine, A. L'Huillier, and M. Lewenstein, *Phys. Rev. Lett.* **77**, 1234 (1996).
- [47] M. Bellini, C. Lyngå, A. Tozzi, M. B. Gaarde, T. W. Hänsch, A. L'Huillier, and C.-G. Wahlström, *Phys. Rev. Lett.* **81**, 297 (1998).
- [48] E. V. van der Zwan, C. C. Chirilă, and M. Lein, *Phys. Rev. A* **78**, 033410 (2008).
- [49] L. V. Keldysh, *Zh. Eksp. Teor. Fiz.* **47**, 1945 (1964) [*Soc. Phys. -JETP* **20**, 1307 (1965)].
- [50] F. H. M. Faisal, *J. Phys. B: At. Mol. Phys.* **6**, L89 (1973).
- [51] H. R. Reiss, *Phys. Rev. A* **22**, 1786 (1980).